Ferromagnetic order of ultra-thin $La_{0.7}Ba_{0.3}MnO_3$ sandwiched between $SrRuO_3$ layers

Cinthia Piamonteze,[1, a)] Francis Bern,[2, b)] Sridhar Reddy Venkata Avula,[1] Michal Studniarek,[1] Carmine Autieri,[3, c)] Michael Ziese,[2] and Ionela Lindfors-Vrejoiu[4]
[1)]*Swiss Light Source, Paul Scherrer Institut, CH-5232 Villigen PSI, Switzerland*
[2)]*Felix-Bloch-Institut für Festkörperphysik Universität Leipzig D-04103 Leipzig, Germany*
[3)]*International Research Centre MagTop, Institute of Physics, Polish Academy of Sciences, Aleja Lotników 32/46, PL-02668 Warsaw, Poland*
[4)]*II. Physikalisches Institut Universität zu Köln D-50937 Köln, Germany*

We demonstrate the stability of ferromagnetic order of one unit cell thick optimally doped manganite ($La_{0.7}Ba_{0.3}MnO_3$, LBMO) epitaxially grown between two layers of $SrRuO_3$ (SRO) by using x-ray magnetic circular dichroism. At low temperature LBMO shows an inverted hysteresis loop due to the strong antiferromagnetic coupling to SRO. Moreover, above SRO T_C the manganite still exhibits magnetic remanence. Density Functional Theory calculations show that coherent interfaces of LBMO with SRO hinder electronic confinement and the strong magnetic coupling enables the increase of the LBMO T_C. From the structural point of view, interfacing with SRO enables LBMO to have octahedral rotations similar to bulk. All these factors jointly contribute for stable ferromagnetism up to 130 K for a one unit cell LBMO film.

Optimally doped manganite ($La_{0.7}Sr_{0.3}MnO_3$ - LSMO) has attracted interest for use in magnetic tunnel junctions due to its high values of spin polarization and Curie temperature (T_C)[1]. However, such applications have been partially hindered, due to findings that T_C strongly decreases for ultra-thin layers, with a non-ferromagnetic insulator layer of about 5 unit cells[2–4]. Several reasons have been attributed for the origin of the magnetic dead layer in manganites. Among them, charge transfer[5], octahedral rotation[6] and symmetry breaking[7] are likely to play a role.

On the other hand superlattices of LSMO with $SrRuO_3$ (SRO) or $La_{0.7}Sr_{0.3}CrO_3$ exhibit ferromagnetism for single LSMO layers down to 2 unit cells (u.c.), corresponding to around 0.8 nm[8,9]. In superlattices composed of antiferromagnetic layers of manganite ($La_{2/3}Ca_{1/3}MnO_3$) and ruthenate ($CaRuO_3$) a ferromagnetic metallic ground state was observed, and attributed to charge transfer at the interface[10]. LSMO and SRO couple antiferromagnetically via the interfacial oxygen 2p states[11] and heterostructures of manganites and ruthenates exhibit a complicated antiferromagnetic structure as a function of field and temperature.[12]. In fact, superlattices combining manganites and ruthenates were proposed candidates for synthetic antiferromagnets[13].

Here we investigate the stability of ferromagnetic order in one u.c.-thick (u.c. = unit cell) $La_{0.7}Ba_{0.3}MnO_3$ (LBMO) interfaced epitaxially with two layers of 3 u.c.-thick $SrRuO_3$ (SRO), grown on $SrTiO_3$ (001) (STO), which will be called 3|1|3 from now on. We have chosen LBMO instead of LSMO, since this has a much better lattice matching with both STO and SRO. The magnetic properties of LBMO and LSMO are however very similar. Using x-ray magnetic circular dichroism (XMCD) we measure element specific magnetization curves, thus being able to investigate the magnetism of LBMO and SRO separately. We show that at low temperature LBMO shows an antiferromagnetic coupling to SRO, as also observed in superlattices through total magnetometry[14]. Interestingly, our data undoubtedly shows that LBMO still exhibits magnetic remanence, even above SRO T_C. To get more insight in the magnetic properties of the 3|1|3 heterostructure, we perform Density Functional Theory (DFT) calculations. Our calculations show that a combination of electronic and atomic structure together with the strong magnetic coupling between SRO and LBMO help stabilizing ferromagnetism in ultra-thin LBMO.

High angle annular dark field imaging and electron energy loss spectroscopy performed with a Cs-corrected scanning transmission electron microscope showed the sharp interface of the systems studied here[15]. The 3|1|3 heterostructure was previously investigated by anomalous Hall effect and SQUID magnetization[15]. The XAS and XMCD spectra for Ru and Mn are shown in figure 1. The measured XAS for Mn in 3|1|3 is in agreement with other published spectra from optimally doped manganites and very similar to the one we have measured for a 30 nm of LBMO (fig. 1(a)). No contribution from Mn^{2+} is seen, which often is visible in ultra thin layers directly grown on STO[16]. The Ru M_3 edge overlaps with Ti $L_{3,2}$ edges. Figure 1(b) shows the comparison of the Ru XAS in 3|1|3 with the one measured for a 30 nm thick SRO film and the Ti $L_{3,2}$ measured in a STO crystal. The measured 3|1|3 Ru XAS can be very well reproduced by a combination of the measured SRO and STO spectra on the same energy range, as shown in figure 1(b).

Figures 1(c) and (d) show the XAS and XMCD measured for Ru and Mn, respectively, measured at 10 K and 6.8 T for 3|1|3 heterostructure. The XMCD signal is proportional to the net magnetic moment projected along the x-ray beam direction. Therefore, two measurement geometries are used for probing different magnetization directions. Normal incidence (NI) measurement probes the out-of-plane axis while grazing incidence measurement (GI) probes predominantly the component of in-plane magnetization. In NI (dashed lines in figure

[a)]Electronic mail: cinthia.piamonteze@psi.ch
[b)]Also at Laboratoire de Physique de la Matière Condensée, École Polytechnique, Palaiseau F-91128, Palaiseau cedex, France
[c)]Also at Consiglio Nazionale delle Ricerche CNR-SPIN, UOS Salerno, 84084 Fisciano (Salerno), Italy

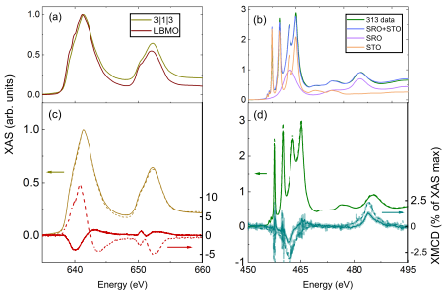

FIG. 1. (a) Mn XAS for 3|1|3 compared to LBMO single layer. (b)Ru XAS measured for the 3|1|3 trilayer (blue) compared to a simulation (blue) of the spectra for 3|1|3 using a combination of the measured data for SRO and STO. The SRO (violet), STO (orange) contributions to the simulated XAS are also shown. The data for 3|1|3 are normalized such that the maximum of SRO contribution is at 1. (c) Mn and (d) Ru XAS (left scale in arbitrary units) and XMCD (right scale in % of the XAS maximum) spectra measured at 10 K and 6.8 T. The continuous lines correspond to measurements in GI and the dashed lines in NI.

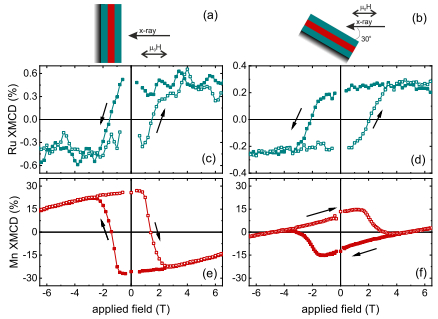

FIG. 2. (a) Measurement geometry sketch for normal and (b) grazing incidence, probing out-of-plane and in-plane magnetization, respectively. (c) SRO hysteresis measured in normal and (d) grazing incidence. (e) LBMO hysteresis measured in normal and (f) grazing incidence. All measurements were performed with the sample at 10 K.

1(c),(d)) Mn and Ru have opposite sign for the XMCD signal evidencing the antiferromagnetic coupling between these two layers. Since SRO has a larger contribution to the total magnetization, the Ru moment is parallel to the field while Mn is opposite to the applied field. The Ru XMCD is about two times larger in NI than in GI, which agrees with the expected out-of-plane easy axis measured in SRO films deposited on STO(001)[17]. On the other hand, the Mn XMCD in GI has the same sign as Ru showing that at high magnetic field both have a component parallel to the applied field. The overall smaller XMCD signals for GI indicates a canted magnetization state.

In order to understand further the field dependence of the individual layers in both geometries, we have measured the XMCD signal as a function of applied field in order to obtain an element specific hysteresis curve. Figure 2 shows the magnetization curves measured at Ru (figure 2 (c) and (d)) and Mn (figure 2 (e) and (f)) resonances as a function of applied magnetic field. Figures 2(c) and (d) show further confirmation for the out-of-plane easy axis in these trilayers: the Ru XMCD signal is larger and the coercive field smaller for the NI measurement compared to GI. The coercive field measured for out-of-plane (figure 2(c)) is ≈ 2.0 T. This is about twice the value measured for a bare 5 nm-thick (≈ 12 u.c.) SRO film[17]. This difference likely comes from the larger contribution of the surface anisotropy in the much thinner SRO layer investigated here as well as a reduced demagnetization field due to the AF configuration. As mentioned before, at GI the largest contribution is from the in-plane magnetization, but an out-of-plane component also contributes to the signal.

The Mn magnetization for the 1 u.c.-thick LBMO for NI (fig. 2(e)) shows a clear inverted hysteresis, evidencing again the antiferromagnetic coupling between optimally doped manganite and SRO[9,11]. Similar inverted hysteresis were measured for thicker LSMO/SRO bilayers using XMCD[18]. Figure 2(e) shows that a single LBMO layer still exhibits ferromagnetic behavior at 10 K. In GI (figure 2(f)), the LBMO layer does not rigidly oppose the SRO magnetization, as in NI. Instead, around 5 T the LBMO film XMCD is close to zero. Above this applied field the Mn magnetization changes sign having a component in the direction of the applied magnetic field. This shows that the Mn-Mn double exchange coupling and the in-plane magnetic anisotropy for LBMO together with the Zeeman energy overcome the antiferromagnetic coupling between Mn and Ru. This is particularly easier at grazing incidence since the Ru magnetic moment component along the field direction is smaller. A quantitative estimation of the magnetic moment is obtained by applying sum rules[19,20] to the XMCD spectra at applied field and in remanence (see the Supplementary Material, SM). For Mn the moments found for 3|1|3 are $1.8(2)\mu_B$ (NI) and $-0.33(5)\mu_B$ (GI) at 6.8 T; $3.1(5)\mu_B$ (NI) and $1.9(3)\mu_B$ (GI) at remanence. For LBMO single film the moment found was $3.4(6)\ \mu_B$. For the SRO single film the moment found was $1.37(7)\mu_B$, in agreement with neutron studies[21]. The Ru moment in SRO was probed by XMCD with a certain disparity in results[22,23]. The sum rules on the 3|1|3 Ru data turned out to have very large error bars due to the uncertainty of the XMCD baselines in comparison to the magnitude of the signal. For this reason we scaled the Ru XMCD for the 3|1|3 to the one for the SRO single film for an estimate of the moment size. The Ru XMCD in 3|1|3 is about 75% of the one in SRO at NI and 40% in GI (see SM).

We model the hysteresis using the magnetic total energy in the semiclassical form of the 6 SRO layers coupled with 1 LBMO layer. We consider the magnetic exchange between the Ru and Mn atoms, the magnetocrystalline anisotropy and

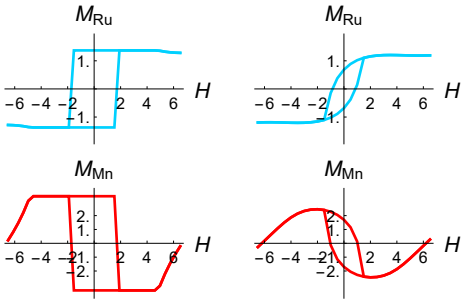

FIG. 3. Same quantities as Fig. 2 using the theoretical results of the semiclassical model. The unit of the magnetization is in μ_B, the unit of the magnetic field is in Tesla. Left hand side graphs are for NI and right hand side graphs are for GI.

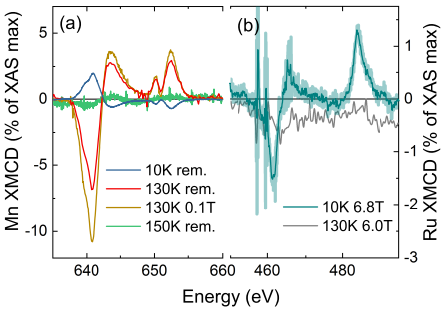

FIG. 4. XMCD measured in grazing incidence at (a) Mn $L_{2,3}$ edges and (b) Ru $M_{2,3}$ edges. Temperature and applied field are indicated in the legend. Remanence (rem.) measurements were performed at no applied field after saturation at 6.0 T.

the interaction between the spin and the magnetic field.

$$E = 2J^{001}_{Ru-Mn}\cos(\theta_{Ru}-\theta_{Mn}) + \\ +6K_{Ru}\cos^2(\theta_{Ru}) + K_{Mn}\cos^2(\theta_{Mn}) + \\ -6M_{Ru}H\cos(\theta_{Ru}-\theta_H) - M_{Mn}H\cos(\theta_{Mn}-\theta_H) \quad (1)$$

where the magnetization of the Ru and Mn atoms are fixed to the experimental values M_{Ru}=1.37 μ_B and M_{Mn}=3.4 μ_B, while K_{Ru} and K_{Mn} are the magnetocrystalline anisotropy for the Ru and Mn spins, respectively. The angles θ_{Ru} and θ_{Mn} are the angles of the spins with respect to the reference system (the film surface in our case). Because of the AFM coupling between Ru and Mn, the θ_{Ru} and θ_{Mn} angles differ by 180 degrees at zero magnetic field and they change with the magnetic field. H and θ_H are the intensity and the angle of the magnetic field, in the experimental setup θ_H=$\frac{\pi}{2}$ and $\frac{\pi}{6}$. We tune the field H, and we calculate θ_{Ru} and θ_{Mn} for the given magnetic field from the minimum of the total energy. For H larger than the coercive field, the Ru moment aligns to the magnetic field and θ_{Ru} becomes equal to θ_H. There is a competition between the 6 layers of SRO and the single layer of LBMO. Since $6m_{Ru} > m_{Mn}$, the dominant behaviour is given by the magnetization of the 6 layers of SRO that follow the magnetic field, as a consequence the LBMO aligns antiparallel to the magnetic field. The competition between $2J^{001}_{Ru-Mn}$ and $M_{Mn}H$ decides the rotation of the Mn layer. The result is displayed in Fig. 3, showing a good agreement with the experiment. The calculations consider a single domain and that could explain the discrepancy of the magnetization for Ru measured in GI. In the experiment clearly not all domains align with the applied field, while in the calculations the single domain does.

Next we look at the temperature dependence of the magnetic behaviour. Figure 4 shows the XMCD data measured in GI at remanence for LBMO at 130 K and 150 K compared to 10 K. The data for SRO at 130 K and applied field is plotted for reference. For technical reasons, it is very difficult to have good signal/noise in the magnetization curve for fields close to zero, making it a challenge to detect hysteresis opening below $\approx$ 50 mT. For this reason, we choose to measure the XMCD in remanence as an evidence for the presence or not of ferromagnetic order. The remanence data are measured at no applied field after saturating the moments at 6 T. The superconducting magnet coil used has remanent field of approximately 10 mT. At 10 K (blue curve in figure 4) the remanence signal for LBMO is opposite to Ru, as expected from the XMCD *vs.* field data shown in figure 2. At 130 K, XMCD signal for Ru is below the detection level, even at 6 T. This is not so surprising since the T_C for SRO in these trilayers is around 100 K, as shown by Bern *et al*[15]. The XMCD signal for LBMO at 0.1 T and 130 K has the opposite sign as for LBMO at 10 K, showing that at this temperature the XMCD for LBMO is parallel to the applied magnetic field. This is an additional evidence that, indeed, SRO is not anymore ferromagnetic and LBMO acts as an independent magnetic layer. When removing the applied field, the Mn XMCD keeps the same sign and is reduced to 67 % of the value at 0.1 T showing a clear magnetic remanence. Therefore, the XMCD data unequivocally shows that even above the T_C for SRO, the single LBMO layer still retains its ferromagnetic ordering. When increasing the temperature to 150 K, the XMCD signal for LBMO is not anymore detectable as shown by the green curve in figure 4(a).

From the DFT calculations, the magnetic configuration of the ground state is represented by the Mn-spins antiparallel to the Ru-spins. The magnetic profile is reported in Fig. 5b) for two sets of Coulomb repulsion. In the first set, we have used the values in the bottom of the typical range (U_{Ru}=0.2 eV, U_{Mn}=3 eV) while in the second set we have used values in top of the typical ranges (U_{Ru}=1 eV, U_{Mn}=6 eV).[24–26] In both cases, we find the largest magnetic moment for the SRO in the inner layers. The average magnetic moment is in the range 0.9-1.3 μ_B for the Ru and 3.6-3.8 μ_B for the Mn; these quantities are strongly dependent on the Coulomb repulsion. Lower values of U_{Mn} will make the theoretical value closer to the 3.4 μ_B experimentally found for the LBMO. The increase in the $T_{C,LBMO}$ due to the presence of the SRO is estimated

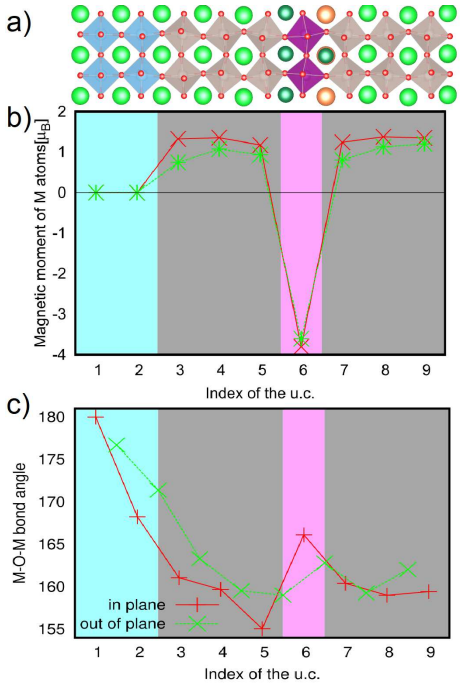

FIG. 5. a) Crystal structure of the 3|1|3 heterostructures obtained after structural relaxation in DFT. We use the same color of the atoms to define the corresponding regions in the bottom figures. b) Magnetic moments of the metal atoms in DFT for U_{Ru}=0.2 eV and U_{Mn}=3 eV (green dashed line) and U_{Ru}=1 eV and U_{Mn}=6 eV (red solid line). The connecting lines are a guide for the eyes. c) In plane and out of plane M-O-M bond angles of the 3|1|3 hetetrostructure in DFT for U_{Ru}=1 eV and U_{Mn}=6 eV. The lines are a guide for the eyes.

in mean field approximation as $\frac{J^{001}_{Mn,Ru}}{2J^{100}_{Mn,Mn}}$, which is of the order of 0.08-0.09. This Ru-Mn magnetic coupling produces an increase of 8-9% of the $T_{C,LBMO}$ with respect to an isolated 1 u.c. of LBMO, in line with the experimental results. Additional contribution to the $T_{C,LBMO}$ could come from the increase in dimensionality. This is indicated by the density of states (see SM), which show that the Ru and Mn bandwidths lie in the same energy range, avoiding the quantum confinement.

We have also looked at octahedral rotations of the 3|1|3 heterostructure. STO with its cubic structure has no octahedral rotation and will likely inhibit the corner sharing octahedral rotation in LBMO. DFT results in Fig. 5c) show how the octahedral distortions behave for the 3|1|3 heterostructure. The in plane M-O-M bond angle in the first layer of STO is theoretically constrained to be 180 degrees. The STO suppresses the octahedral rotations of the layers interfaced with it, but going away from STO the octahedral rotations increase. Despite the large octahedral rotations of the SRO, we can observe that in the LBMO region the octahedral rotations are comparable with bulk values of LBMO. Therefore, the SRO prevents the reduction in critical temperature via structural effects.

In summary our results show that one u.c. thick LBMO has a T_C between 130 K and 150 K when epitaxially interfaced with two adjacent 3 u.c. thick SRO layers. This shows greatly improved ferromagnetic properties compared to a bare ultra-thin film of optimally doped manganite. DFT calculations show that interfacing with SRO adjacent layers provides a 3D electronic structure to the LBMO, hindering quantum confinement effects. The strong Ru-Mn magnetic coupling also enhances LBMO T_C even when SRO is already in the paramagnetic phase. In addition SRO favorably acts like a buffer that enables LBMO octahedral rotation close to bulk values. All these effects combined contribute to the stable ferromagnetic state for LBMO. The results reported here demonstrate how impactful epitaxial growth is for the physical properties of perovskite oxides and that effective engineering of the properties can be obtained by suitable choice of the substrate and buffer layers. We found a particular solution for the design of ferromagnetically stable ultra-thin epitaxial films, showing that there exist possibilities to circumvent the notorious dead layer effect that has been thought to annihilate the ferromagnetic order in ultra-thin manganite layers.

SUPPLEMENTARY MATERIAL

See supplementary material for additional information on film growth, computational details and XMCD measurement conditions as well as the XMCD sum rules.

ACKNOWLEDGMENTS

C. A. is supported by the Foundation for Polish Science through the International Research Agendas program co-financed by the European Union within the Smart Growth Operational Programme. C. A. acknowledges the access to the computing facilities of the Interdisciplinary Center of Modeling at the University of Warsaw, Grant No. G73-23 and G75-10. C. A. acknowledges the CINECA award under the IsC81 "DISTANCE" Grant for the availability of high-performance computing resources and support. I.L.-V. thanks Gennady Logvenov and Georg Cristiani for the use of the PLD system for the sample fabrication. S. R. V. A. thanks funding from the Swiss National Science Foundation, grants 2000-0_192393 and 200021_169467.

DATA AVAILABILITY

The data that support the findings of this study are available from the corresponding author upon reasonable request.

[1] J. H. Park, E. Vescovo, H. J. Kim, C. Kwon, R. Ramesh, and T. Venkatesan, "Direct evidence for a half-metallic ferromagnet," Nature **392**, 794–796 (1998).

[2] M. Bibes, L. Balcells, S. Valencia, J. Fontcuberta, M. Wojcik, E. Jedryka, and S. Nadolski, "Nanoscale Multiphase Separation at $La_{2/3}Ca_{1/3}MnO_3/SrTiO_3$ Interfaces," Phys. Rev. Lett. **87**, 545 (2001).

[3] M. Huijben, L. W. Martin, Y.-H. Chu, M. B. Holcomb, P. Yu, G. Rijnders, D. H. A. Blank, and R. Ramesh, "Critical thickness and orbital ordering in ultrathin $La_{0.7}Sr_{0.3}MnO_3$ films," Phys. Rev. B **78**, 094413 (2008).

[4] L. Chen, Z. Wang, G. Wang, H. Guo, M. Saghayezhian, Z. Liao, Y. Zhu, E. W. Plummer, and J. Zhang, "Surface and interface properties of $La_{2/3}Sr_{1/3}MnO_3$ thin films on $SrTiO_3$(001) ," Phys. Rev. Materials **3**, 044407 (2019).

[5] H. Yamada, Y. Ogawa, Y. Ishii, H. Sato, M. Kawasaki, H. Akoh, and Y. Tokura, "Engineered Interface of Magnetic Oxides," Science **305**, 646–648 (2004).

[6] E. J. Moon, P. V. Balachandran, B. J. Kirby, D. J. Keavney, R. J. Sichel-Tissot, C. M. Schlepütz, E. Karapetrova, X. M. Cheng, J. M. Rondinelli, and S. J. May, "Effect of Interfacial Octahedral Behavior in Ultrathin Manganite Films," Nano Lett. **14**, 2509–2514 (2014).

[7] S. Valencia, L. Peña, Z. Konstantinovic, L. Balcells, R. Galceran, D. Schmitz, F. Sandiumenge, M. Casanove, and B. Martínez, "Intrinsic antiferromagnetic/insulating phase at manganite surfaces and interfaces," J. Phys.: Cond. Mat. **26**, 166001 (2014).

[8] S. Koohfar, A. B. Georgescu, I. Hallsteinsen, R. Sachan, M. A. Roldan, E. Arenholz, and D. P. Kumah, "Effect of strain on magnetic and orbital ordering of $LaSrCrO_3/LaSrMnO_3$ heterostructures," Phys. Rev. B **101**, 064420 (2020).

[9] M. Ziese, F. Bern, E. Pippel, D. Hesse, and I. Vrejoiu, "Stabilization of Ferromagnetic Order in $La_{0.7}Sr_{0.3}MnO_3$–$SrRuO_3$ Superlattices," Nano Lett. **12**, 4276–4281 (2012).

[10] P. F. Chen, B. B. Chen, X. L. Tan, H. R. Xu, X. F. Xuan, Z. Guo, F. Jin, and W. B. Wu, "High-T_C ferromagnetic order in $CaRuO_3/La_{2/3}Ca_{1/3}MnO_3$ superlattices," Appl. Phys. Lett. **103**, 262402 (2013).

[11] Y. Lee, B. Caes, and B. N. Harmon, "Role of Oxygen 2p states for antiferromagnetic interfacial coupling and positive exchange bias of ferromagnetic LSMO/SRO bilayers," J. Alloy. Compd. **450**, 1–6 (2008).

[12] Z. Huang, Ariando, X. Renshaw Wang, A. Rusydi, J. Chen, H. Yang, and T. Venkatesan, "Interface Engineering and Emergent Phenomena in Oxide Heterostructures," Adv. Mater. **30**, 1802439 (2018).

[13] B. Chen, H. Xu, C. Ma, S. Mattauch, D. Lan, F. Jin, Z. Guo, S. Wan, P. Chen, G. Gao, F. Chen, Y. Su, and W. Wu, "All-oxide–based synthetic antiferromagnets exhibiting layer-resolved magnetization reversal ," Science **357**, 191–194 (2017).

[14] M. Ziese, I. Vrejoiu, E. Pippel, P. Esquinazi, D. Hesse, C. Etz, J. Henk, A. Ernst, I. V. Maznichenko, W. Hergert, and I. Mertig, "Tailoring Magnetic Interlayer Coupling in $La_{0.7}Sr_{0.3}MnO_3/SrRuO_3$ Superlattices," Phys. Rev. Lett. **104**, 167203 (2010).

[15] F. Bern, M. Ziese, I. Vrejoiu, X. Li, and P. A. van Aken, "Magnetic and magnetotransport properties of ultrathin $La_{0.7}Ba_{0.3}MnO_3$ epitaxial films embedded in $SrRuO_3$," New J. Phys. **18**, 053021 (2016).

[16] J. S. Lee, D. A. Arena, P. Yu, C. S. Nelson, R. Fan, C. J. Kinane, S. Langridge, M. D. Rossell, R. Ramesh, and C. C. Kao, "Hidden Magnetic Configuration in Epitaxial $La_{1-x}Sr_xMnO_3$ Films," Phys. Rev. Lett. **105**, 257204 (2010).

[17] M. Ziese, I. Vrejoiu, and D. Hesse, "Structural symmetry and magnetocrystalline anisotropy of $SrRuO_3$ films on $SrTiO_3$," Phys. Rev. B **81**, 184418 (2010).

[18] S. Das, A. D. Rata, I. V. Maznichenko, S. Agrestini, E. Pippel, N. Gauquelin, J. Verbeeck, K. Chen, S. M. Valvidares, H. B. Vasili, J. Herrero-Martin, E. Pellegrin, K. Nenkov, A. Herklotz, A. Ernst, I. Mertig, Z. Hu, and K. Dörr, "Low-field switching of noncollinear spin texture at $La_{0.7}Sr_{0.3}MnO_3$-$SrRuO_3$ interfaces," Phys. Rev. B **99**, 024416 (2019).

[19] B. T. Thole, C. Paaolo, F. Sette, and G. van der Laan, "X-Ray Circular Dichroism as a Probe of Orbital Magnetization," Phys. Rev. Lett. **68**, 1943–1946 (1992).

[20] P. Carra, B. T. Thole, M. Altarelli, and X. Wang, "X-Ray Circular Dichroism and Local Magnetic Fields," Phys. Rev. Lett. **70**, 694–697 (1993).

[21] S. Lee, J. R. Zhang, S. Torii, S. Choi, D.-Y. Cho, T. Kamiyama, J. Yu, K. A. McEwen, and J.-G. Park, "Large in-plane deformation of RuO_6 octahedron and ferromagnetism of bulk $SrRuO_3$," J. Phys.: Condens. Matter **25**, 465601 (2013).

[22] S. Agrestini, Z. Hu, C.-Y. Kuo, M. W. Haverkort, K.-T. Ko, N. Hollmann, Q. Liu, E. Pellegrin, M. Valvidares, J. Herrero-Martin, P. Gargiani, P. Gegenwart, M. Schneider, S. Esser, A. Tanaka, A. C. Komarek, and L. H. Tjeng, "Electronic and spin states of $SrRuO_3$ thin films: An x-ray magnetic circular dichroism study," Phys. Rev. B **91**, 075127 (2015).

[23] J. Okamoto, T. Okane, Y. Saitoh, K. Terai, S.-I. Fujimori, Y. Muramatsu, K. Yoshii, K. Mamiya, T. Koide, A. Fujimori, Z. Fang, Y. Takeda, and M. Takano, "Soft x-ray magnetic circular dichroism study of $Ca_{1-x}Sr_xRuO_3$ across the ferromagnetic quantum phase transition," Phys. Rev. B **76**, 479 (2007).

[24] S. Roy, C. Autieri, B. Sanyal, and T. Banerjee, "Interface control of electronic transport across the magnetic phase transition in $SrRuO_3/SrTiO_3$ heterointerface," Sci. Rep. **5**, 15747 (2015).

[25] C. Autieri and B. Sanyal, "Unusual ferromagnetic $YMnO_3$ phase in $YMnO_3/La_{2/3}Sr_{1/3}MnO_3$ heterostructures," New J. Phys. **16**, 113031 (2014).

[26] S. Keshavarz, Y. O. Kvashnin, D. C. M. Rodrigues, M. Pereiro, I. Di Marco, C. Autieri, L. Nordström, I. V. Solovyev, B. Sanyal, and O. Eriksson, "Exchange interactions of $CaMnO_3$ in the bulk and at the surface," Phys. Rev. B **95**, 115120 (2017).

Applied Physics Letters

PLEASE CITE THIS ARTICLE AS DOI: 10.1063/5.0043057

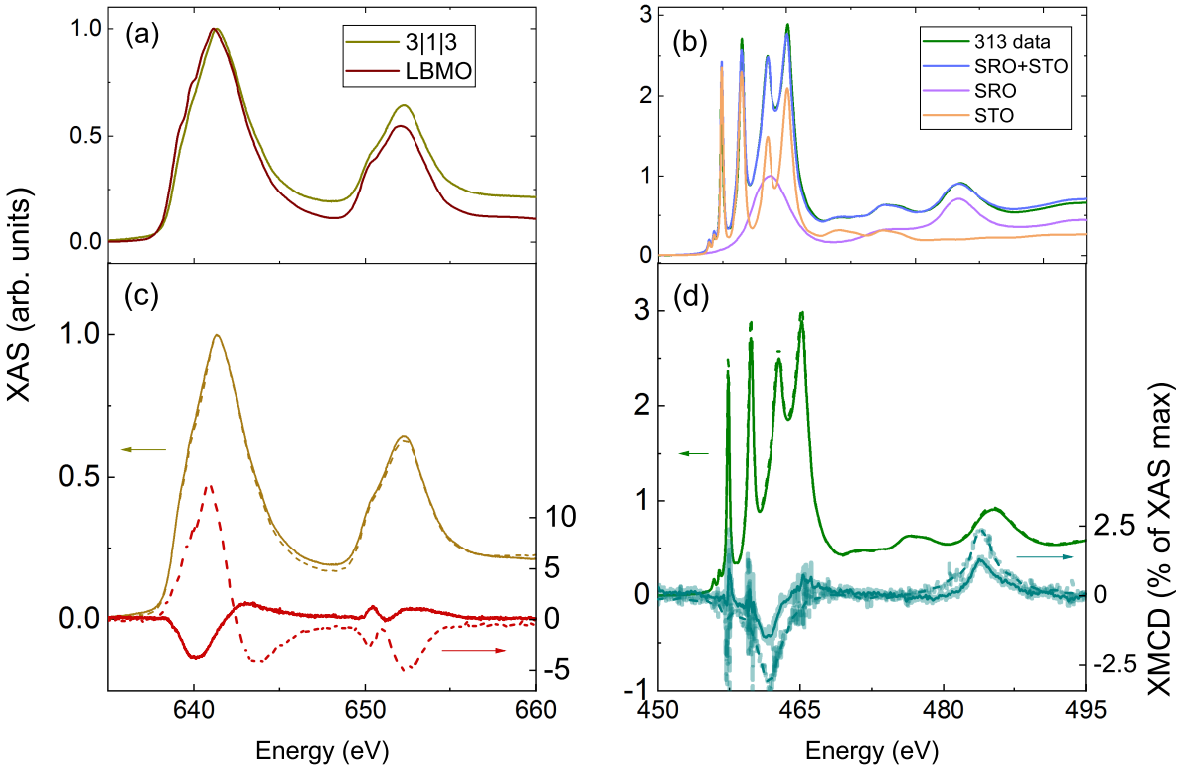

PLEASE CITE THIS ARTICLE AS DOI: 10.1063/5.0043057

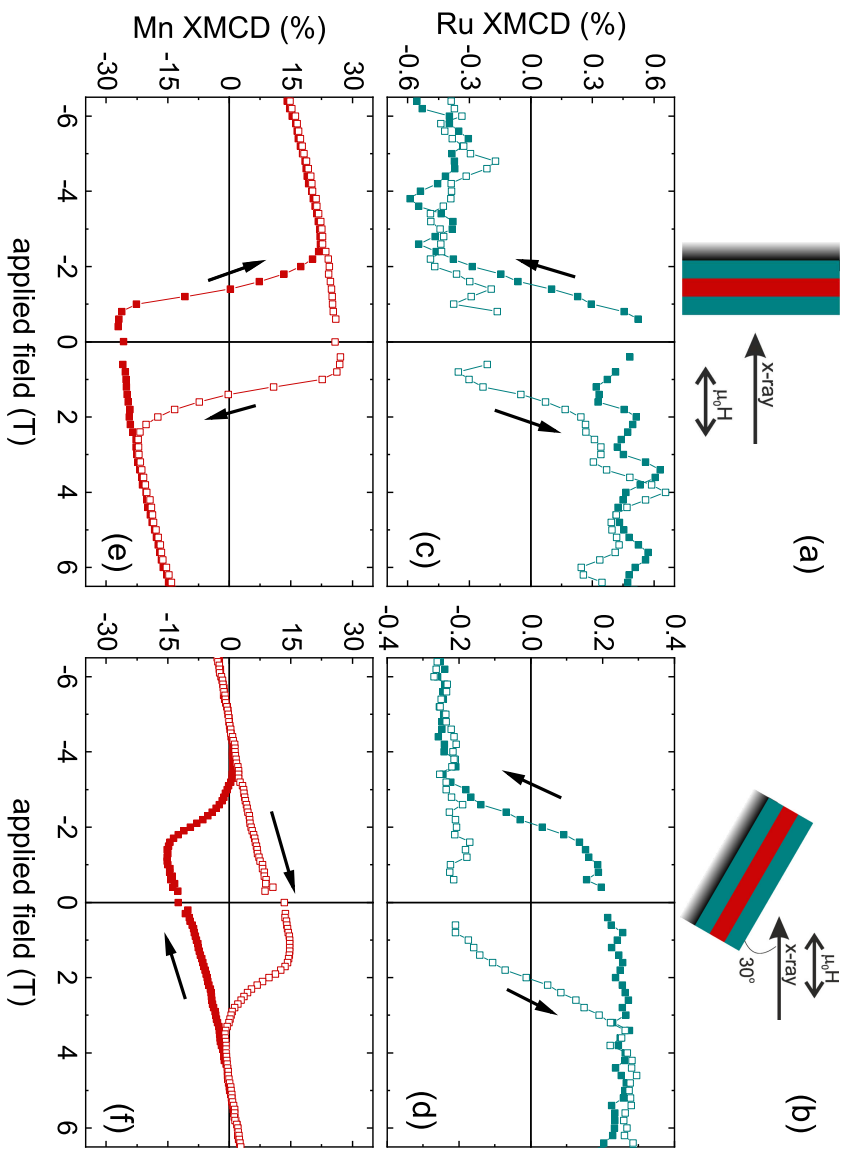

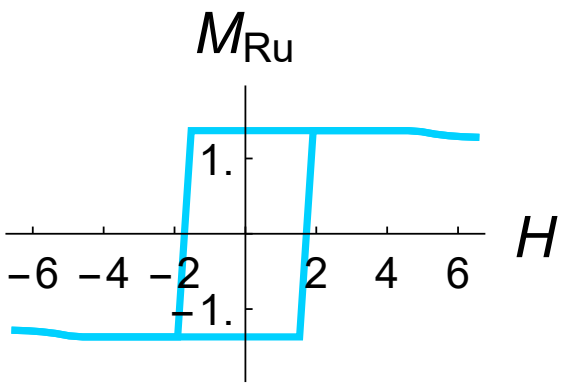

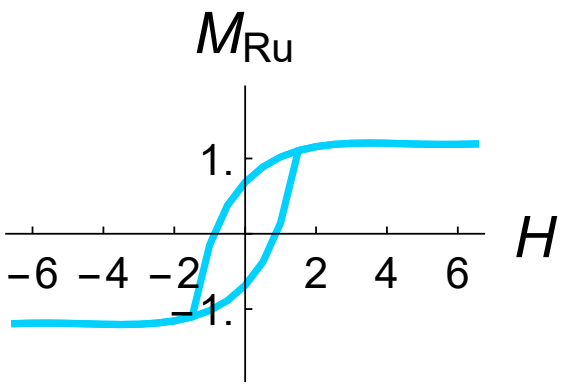

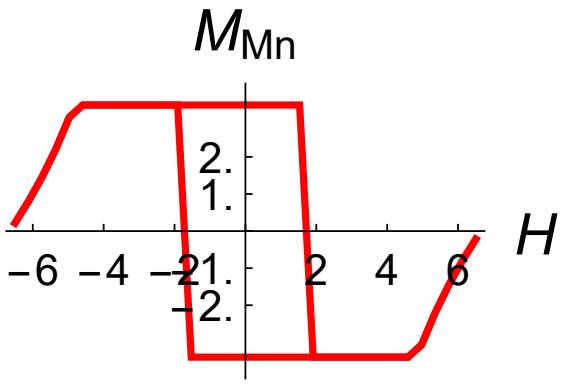

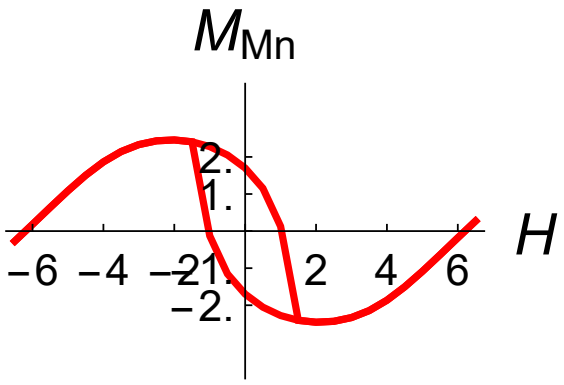

PLEASE CITE THIS ARTICLE AS DOI: 10.1063/5.0043057

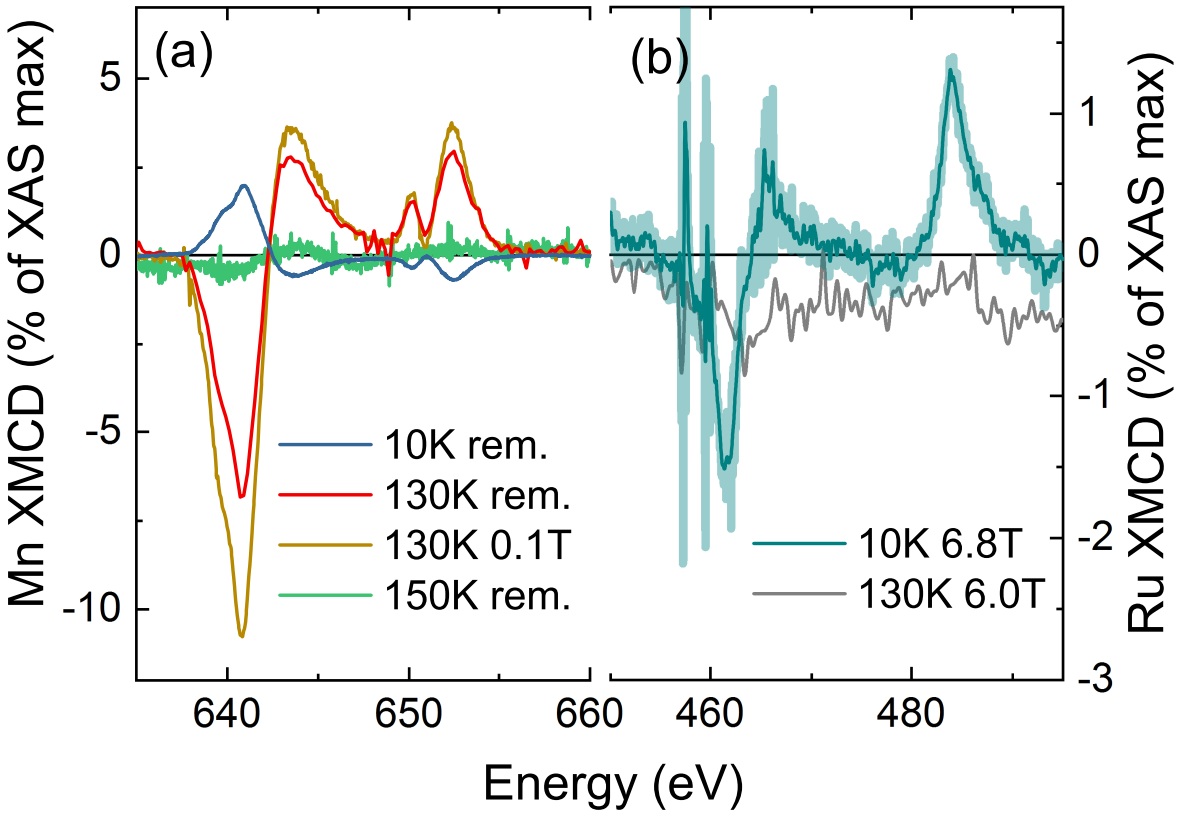

PLEASE CITE THIS ARTICLE AS DOI: 10.1063/5.0043057